Low-Temperature Synthesis of Co-Doped SnSe

Nojus Medzelas

s4123808

Bachelor's Thesis

BSc Chemistry

Zernike Institute for Advanced Materials, Faculty of Science and Engineering

University of Groningen

First assessor: Dr. G.R. Blake

Second assessor: Prof. B. Noheda

Supervisor: Xin Feng

Research Group: Solid State Materials for Electronics

July 2025

Abstract

In this thesis, a hydrothermal synthesis method of SnSe was investigated and optimized for cobalt doping. Post-synthesis aqueous autoclave doping proved most effective in producing a clean product. Powder XRD confirmed the orthorhombic SnSe phase with minor secondary phases, namely SnO_2 and elemental cobalt. SEM and EDAX were used to confirm the typical microplate morphology and homogeneous Co distribution. Magnetic measurements revealed paramagnetic behavior with negative Weiss temperatures and unexpectedly large effective moments for Co. The data suggest that Co nanoclusters were formed, which could give rise to superparamagnetic properties. However, further analysis is needed to clarify the findings, especially the nature of the cobalt species.

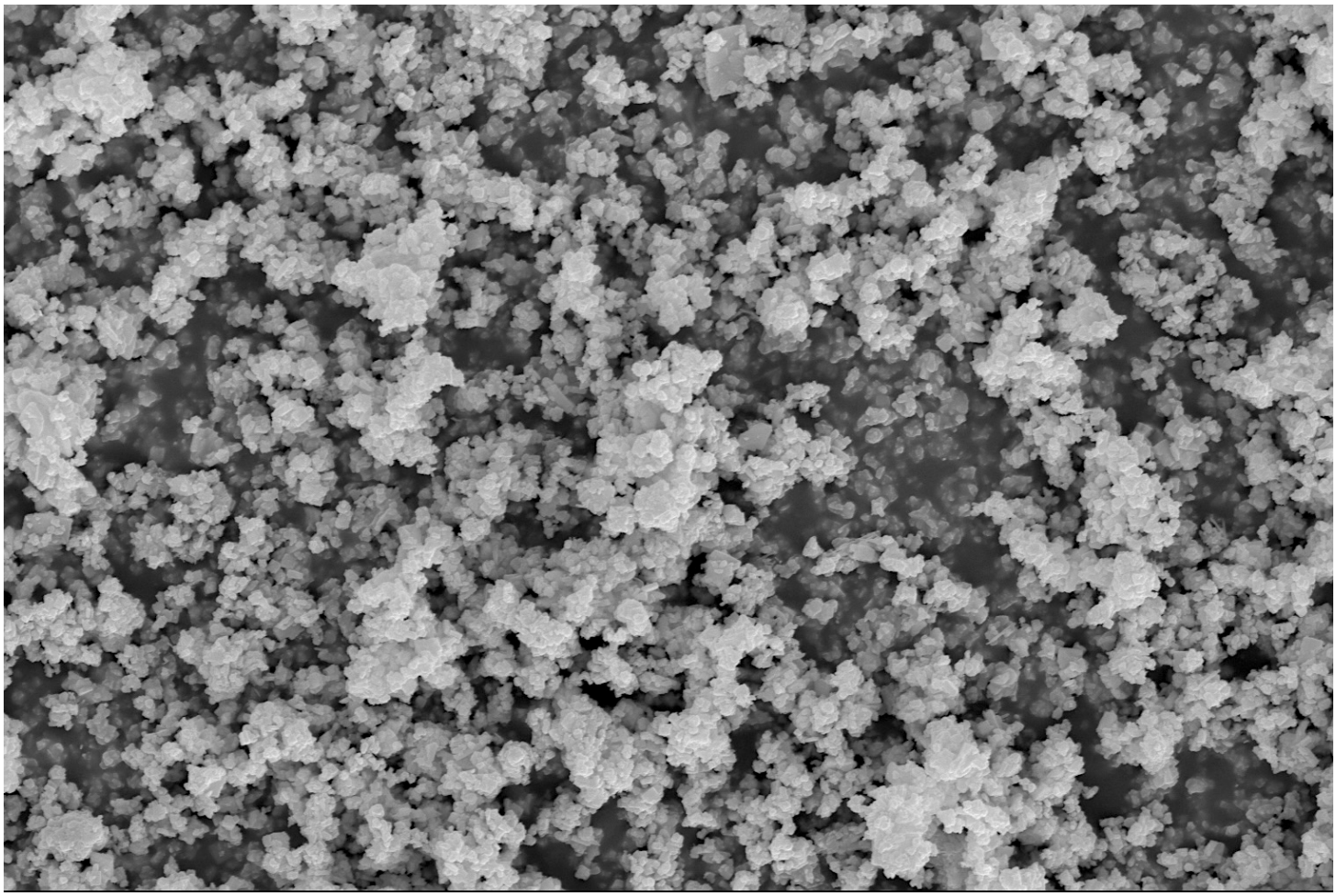

Table of Contents

1 Introduction

In recent decades, scientists have been increasingly focused on environmentally friendly advancements due to sustainability concerns. One significant area is in the capture and reuse of heat that would otherwise be lost to the environment. Thermoelectric materials have gained interest because of their inherent ability to convert heat into electricity. These materials can also be used for refrigeration via the opposite effect.[1]

1.1 The Thermoelectric Effect

The thermoelectric effect consists of three interconnected effects: the Seebeck effect, the Peltier effect, and the Thomson effect.

The Seebeck effect refers to the formation of an electrical potential across a material in response to a temperature gradient. This occurs because the majority charge carriers migrate toward the cooler side of the material, due to diffusion, creating a voltage known as the Seebeck voltage.[2] The Seebeck coefficient quantifies this effect - it measures how effectively a material converts a temperature gradient into a voltage. It is defined as the ratio of the voltage difference to the temperature difference. Thermoelectrics are especially appealing because they often rely solely on solid-state components, which contributes to compact device design, the absence of moving parts, silent operation, and long-term reliability.[3]

The Peltier effect is the reverse effect: applying a voltage induces heat flow. Reversing the current direction changes the direction of heat flow. In thermoelectric applications, the Peltier coefficient measures the efficiency of this process. It is quantified by the ratio of heat (Q) to current (I).

The Thomson effect is less understood, although it is important for thermoelectric performance. It describes how a material with a temperature gradient and a current flowing through it will either absorb or emit heat. The Thomson effect sets limits on the temperature gradient and the strength of current that can be applied in thermoelectric systems.[2]

The overall efficiency of a thermoelectric material is often expressed through a dimensionless figure of merit (ZT), defined as:

$$Equation\ 1: \quad ZT = \frac{S^2 \sigma T}{\kappa}$$

where S, σ, T, κ are the Seebeck coefficient, electrical conductivity, absolute temperature, and the total thermal conductivity, comprising both electronic and lattice components, respectively. Maximizing ZT requires simultaneously enhancing the power factor $S^2\sigma$ while minimizing κ. This interplay presents a materials design challenge, as these parameters are often interdependent.

1.2 Tin Selenide as a Thermoelectric Material

Tin selenide (SnSe) has emerged as a highly promising candidate for cost-effective, environmentally friendly, and scalable thermoelectric applications. This is primarily due to its intrinsically low lattice thermal conductivity and a suitable band gap of approximately 0.9 eV, both of which contribute to a high power factor.[1] Single-crystal SnSe samples have been shown to exhibit very high figures of merit, with ZT values approaching 3. However, polycrystalline SnSe, which is more practical for large-scale synthesis, generally exhibits lower ZT values, ranging from 1 to 1.5, although these values are increasing.[2]

The focus of this thesis is on developing a suitable synthesis route for creating a doped polycrystalline SnSe sample, a step that is crucial for improving scalability and ZT. Bulk materials often allow for simpler and faster synthesis techniques. Cobalt was selected as the dopant due to its magnetic properties and ionic size. Cobalt exhibits a permanent magnetic spin, and if substituted into the SnSe lattice in place of Sn^{2+} ions, it could enhance phonon scattering by disrupting lattice symmetry. This would reduce lattice thermal conductivity and could potentially enhance thermoelectric performance.[4] Furthermore, cobalt has an ionic size smaller, although similar to that of tin, making it structurally compatible. Its high spin value may also contribute to increased spin entropy. Cobalt is relatively abundant, non-toxic when incorporated into the structure, and economically viable. However, caution is necessary as cobalt salts used in synthesis can pose health hazards if not handled correctly.[5]

Several synthesis variables must be optimized to improve the figure of merit. In this work, the synthesis optimization was focused on particle size and vacancy concentration, as particle size in polycrystalline materials directly affects electrical conductivity and thermal behavior after pellet pressing. Additionally, vacancy engineering plays a key role, as vacancies can improve phonon scattering and further reduce thermal conductivity. If the vacancies are filled with cobalt atoms, the magnetic interactions between cobalt and neighboring atoms can increase phonon scattering due to higher spin entropy in the lattice.[2]

Both hydrothermal and solvothermal synthesis routes were considered, although the hydrothermal method was preferred due to its simplicity and the absence of toxic solvents, which are usually necessary in solvothermal techniques.

1.3 Reaction Considerations

The synthesis involves preparing two solutions under an inert atmosphere to prevent the oxidation of reagents. The reagents are prepared in separate containers to maintain an excess of Sn^{2+} ions upon mixing, which minimizes the formation of $SnSe_2$ and other undesired side products.[1] In the first step, $SnCl_2 \cdot 2H_2O$ is dissolved in a basic aqueous solution to yield Sn^{2+}.

$$SnCl_2 \cdot 2H_2O + 4OH^- \rightarrow [Sn(OH)_4]^{2-} + 2Cl^- + 2H_2O \quad (1)$$

Reaction 1 illustrates that a high Sn:NaOH ratio is essential, as lower ratios may lead to precipitation of $Sn(OH)_2$, thereby reducing the availability of Sn^{2+} ions.

In a separate container, elemental selenium (Se) pellets are combined with a small amount of NaOH. Sodium borohydride ($NaBH_4$) is added gradually to reduce selenium. Two competing reactions are proposed.[6]

$$2Se + 4NaBH_4 + 7H_2O \rightarrow 2NaHSe + Na_2B_4O_7 + 14H_2 \quad (2.1)$$

$$Se + (BH_4)^- \rightarrow Se^{2-} + BH_3 + H^+ \quad (2.2)$$

Reactions 2.1 and 2.2 outline the possible competing mechanisms, as Se^{2-} is colorless while NaHSe has a faint yellow color, and both mechanisms result in gas emission. These changes were observed during synthesis. Upon mixing the two solutions, tin and selenium react to form tin selenide.[6]

$$Sn^{2+} + NaHSe \rightarrow SnSe + Na^+ + H^+ \quad (3.1)$$

$$Sn^{2+} + Se^{2-} \rightarrow SnSe \quad (3.2)$$

Reactions 3.1 and 3.2 describe the proposed mechanism of SnSe formation. The ions can either react directly or $(HSe)^-$ can disproportionate to then react according to Reaction 3.2. To minimize the oxidation of the reduced species, exposure to air must be avoided during all of the steps. Sn^{2+} is easily oxidized to Sn^{4+}, leading to SnO_2 precipitation. Similarly, Se^{2-} is unstable in air and oxidizes first to Se^- and then to elemental Se, which is unreactive under these conditions.[7]

1.4 Analysis Techniques

Powder X-ray diffraction (XRD) was used to evaluate the phase purity and crystalline structure of the synthesized samples. The technique enables identification of the main phase by comparing the diffraction pattern to known reference data, as well as the detection of any secondary phases indicative of incomplete reaction or impurities.
To further analyze the crystal structure, Le Bail refinement was applied to the diffraction data. This whole-pattern fitting technique allows accurate extraction of unit cell parameters without requiring prior knowledge of atomic positions. By refining the peak positions and peak shapes, structural information such as lattice parameters can be obtained with high precision. This was particularly important for determining whether doping introduced changes to unit cell dimensions, which would suggest successful incorporation of dopant ions into the SnSe lattice.[8] A Bruker D8 Endeavor measurement system was used with Cu Kα (λ = 1.5406 Å).

Magnetic measurements were carried out using a Physical Property Measurement System (PPMS) to investigate the potential magnetic effects of cobalt doping in SnSe. Measurements were performed on pure and doped SnSe to determine whether cobalt was incorporated and whether it changed the magnetic behavior. The magnetic response was analyzed in terms of magnetic susceptibility (χ) and magnetization (M). Susceptibility is a measure of how much a material is magnetized after being exposed to an external field. Elements with unpaired electrons usually follow the Curie or Curie-Weiss law and exhibit paramagnetic behavior.

$$\text{Equation 2:} \quad \chi = \frac{C}{T - \Theta}$$

Here, C is the Curie constant, T is the temperature, and Θ is the Weiss constant. The Curie constant is a material-specific parameter that is proportional to the square of the effective magnetic moment of the magnetic ions and the number of magnetic centers per unit volume. It reflects how strongly a material responds to an external magnetic field at a given temperature. The Weiss constant (Θ), on the other hand, indicates the presence and nature of magnetic interactions between spins. A positive Θ value suggests ferromagnetic interactions, a negative θ implies antiferromagnetic interactions, and a Θ value close to zero suggests the material behaves as a paramagnet with negligible spin–spin interactions.[9] In this study, any observed changes in magnetic susceptibility between undoped and doped samples were used as evidence for the successful incorporation of cobalt ions. Since cobalt contains unpaired electrons, its introduction into SnSe should introduce paramagnetic properties, which can be measured through magnetic measurements.

Scanning Electron Microscopy (SEM) was used to examine the morphology and grain structure of both doped and undoped SnSe samples. SEM provides high-resolution surface imaging by scanning the sample with a focused electron beam, allowing for direct observation of grain size, surface texture, and morphology. These characteristics are critical for evaluating the quality of thermoelectric materials, where grain boundaries can significantly influence both electrical and thermal transport. To complement the morphological analysis, Energy-Dispersive X-ray Spectroscopy (EDAX) was used for elemental mapping and semi-quantitative elemental analysis. EDAX detects X-rays emitted from the sample as a result of electron beam interaction, enabling identification of the elements and their spatial distribution. This is particularly important for confirming the successful incorporation of cobalt in doped samples and determining whether the dopants are homogeneously distributed or clustered.[10]

2 Methodology

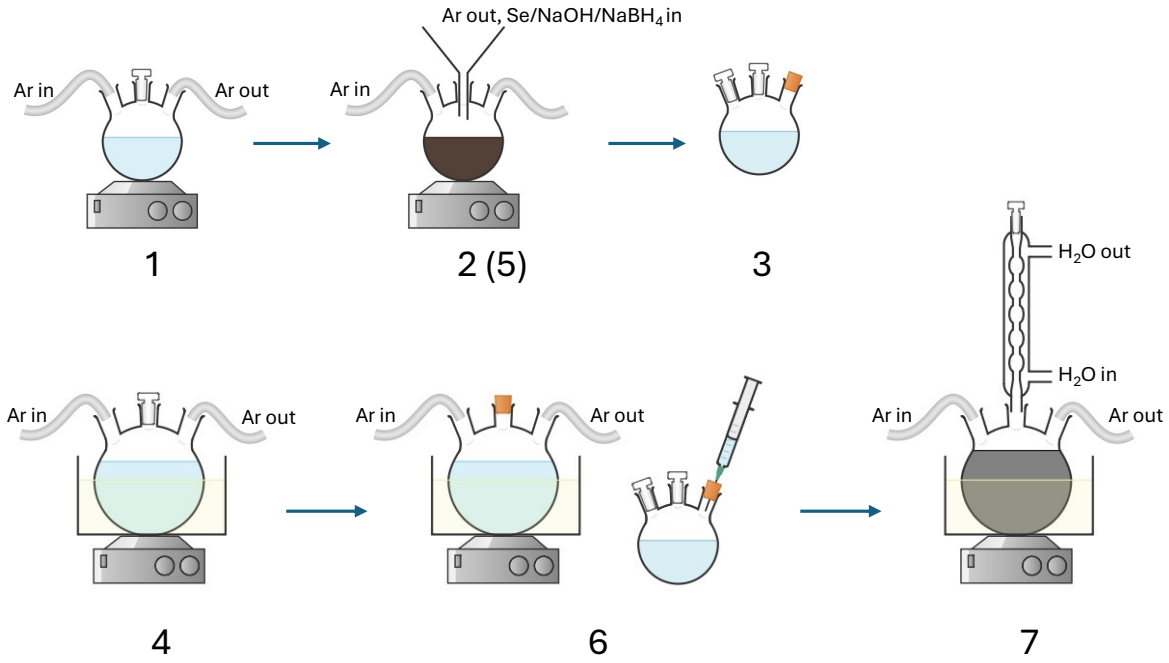

Figure 1: General synthesis setup. Steps 1-3 for selenium source, steps 4-7 for tin source, and SnSe formation. **Diagram made with Chemix.org**

All syntheses were done using two or more precursor solutions, typically involving a selenium source reduced by sodium borohydride ($NaBH_4$) and a tin source in a basic solution. Cobalt was introduced either during SnSe formation or afterwards in a separate doping step. Most syntheses involved heating to around 100 °C and included multiple centrifuge washing steps using water and ethanol mixtures. In the final syntheses, doping was performed in an autoclave after SnSe was initially synthesized.

Reactions were performed under an inert argon atmosphere to avoid oxidation. The process involved first removing oxygen from the solution mixture as shown in Figure 1 (step 1). To add solids, argon flow was increased, and the stopper was replaced by a funnel (step 2). The selenium solution was then sealed with a rubber stopper. Due to the larger volume of Solution 2, an oil bath was used for the tin precursor solution, and the solvent was deoxygenated (step 4). The solids were added in step 5 in the same manner as in step 2. In some cases, $CoCl_2*6H_2O$ was introduced during step 5. The precursor mixtures were combined through the rubber stoppers using a syringe (step 6). The mixture was heated by either adding a stopper or a reflux condenser (step 7).

Table 1: Summary of the attempted doping methods.

Synthesis	Solvent System	Heating Conditions	Washing Procedure	Doping Method	Outcome
1	1. Water, basic (Sn, Co) 2. Water, basic (Se, $NaBH_4$)	100 °C	-	Cobalt dissolved in solution during SnSe formation	$Co(OH)_2$ formed, product discarded
2	1. Ethylene glycol (Sn, Co) 2. Water, basic (Se, $NaBH_4$)	100 °C, 2 h	> 12 washings, alternating between 4:1 and 1:4 EtOH and H_2O, minimal NaCl, minimal acetone, boiling in 0.1M NaOH	Cobalt dissolved in solution during SnSe formation	Poor settling during washing, most product lost during washing
3	1. Ethylene glycol (Sn) 2. Water (Se, $NaBH_4$) 3. Water + ethylene glycol (Co)	100 °C reflux overnight	> 12 washings, alternating between 4:1 and 1:4 EtOH and H_2O	Introduction of Co solution shortly after SnSe formation	Poor settling during washing, contaminants persisted
4	1. Ethylene glycol (Sn) 2. Water (Se, $NaBH_4$) 3. Water + ethylene glycol (Co)	100 °C reflux overnight	11 washing steps, alternating between 4:1 and 1:4 EtOH and H_2O, addition of NaOH when product not settling	Introduction of Co solution shortly after SnSe formation	Poor settling and high product loss during washing, contaminants persisted.
5	1. Water, basic (Sn, Co) 2. Water, basic (Se, $NaBH_4$) 3.1. and 3.2 Water (SnSe, Co) 3.3. Ethylene glycol (SnSe, Co)	100 °C reflux overnight 3.1. and 3.2 Autoclave 130°C, 12h 3.3. Autoclave 220°C, 48h	SnSe 6 washings, alternating between 4:1 and 1:4 EtOH and H_2O 3.1. and 3.2. and 3.3. 3 washings. 80% ethanol, 80% water, then 50% ethanol	Synthesis of SnSe. Post-synthesis Co doping withing an autoclave	Clean product, accidental post-synthesis contamination
6	1. Water, basic (Sn, Co) 2. Water, basic (Se, $NaBH_4$) 3.1. and 3.2 Water (SnSe, Co)	100 °C reflux 30min 3.1. and 3.2 Autoclave 130°C, 80h	SnSe 3 washings, water, 10% EtOH, 10% EtOH 3.1. and 3.2. 5 washings alternating between 4:1 and 1:4 EtOH and H_2O, then 3 washings 50% EtOH	Synthesis of SnSe. Post-synthesis Co doping withing an autoclave	Good yield, clean product

Synthesis 1

The first synthesis involved two basic aqueous solutions. Solution 1 contained 1.2 g NaOH, 1.0 g Se, and 1.0 g $NaBH_4$ in 100 mL of water. $NaBH_4$ was added gradually over four hours while the solution was heated, resulting in a clear solution. Solution 2 was prepared by dissolving 5.0 g NaOH and 2.8 g $SnCl_2 \cdot 2H_2O$ in 300 mL of water. Once clear, 0.308 g of $CoCl_2 \cdot 6H_2O$ was added, forming a pale pink solution and white precipitate, likely $Co(OH)_2$. When the solutions were mixed, a black precipitate formed immediately. Due to the formation of unwanted $Co(OH)_2$, this product was discarded.

Synthesis 2

In the second synthesis, Solution 1 was prepared in a similar way to Synthesis 1, using 0.92 g NaOH, 0.982 g Se, and 1.02 g $NaBH_4$ in 100 mL of water. The solution was heated to around 80 °C. It turned yellow and developed a reddish tint, likely indicating some oxidation. Solution 2 involved dissolving 2.86 g of $SnCl_2 \cdot 2H_2O$ and 1.0007 g of $CoCl_2 \cdot 6H_2O$ in 20 mL of ethylene glycol, followed by the addition of 100 mL of water. The resulting mixture was purple, and a white precipitate (likely undissolved $SnCl_2$) persisted. The two solutions were combined and heated to 100 °C for 2 hours, resulting in black precipitation. Extensive washing was required due to poor settling, with over 12 steps alternating between ethanol and

water. To aid in settling, small amounts of NaCl, acetone, and NaOH were added, although the washed solution only became colorless after boiling the product in 1M NaOH. Most of the product was lost during this process.

Synthesis 3

Synthesis 3 followed a similar procedure but without the addition of NaOH in Solution 1. Here, 0.9616 g of Se and 1.2521 g of $NaBH_4$ were dissolved in 100 mL of water. The mixture was heated to 80 °C, becoming faintly yellow after 2.5 hours. Solution 2 was made by dissolving 2.795 g of $SnCl_2 \cdot 2H_2O$ in 30 mL of ethylene glycol. Solution 3 involved the addition of 0.3032 g of $CoCl_2 \cdot 6H_2O$ in 5 mL water and 5 mL ethylene glycol. Solution 1 was added to Solution 2, followed by 100 mL of water. After stirring for 15 minutes, Solution 3 was added. The mixture was refluxed overnight at 100 °C. The resulting product showed poor settling and remained contaminated with yellow/orange particles after more than 10 washing steps.

Synthesis 4

This synthesis followed the same procedure as Synthesis 3 but with modified reagent quantities and washing procedure. Into Solution 1, 0.9640 g Se and 1.2945 g $NaBH_4$, as well as 100 mL of water, were added. Solution 2 was composed of 2.756 g $SnCl_2 \cdot 2H_2O$ in 30 mL ethylene glycol, and Solution 3 included 0.1755 g $CoCl_2 \cdot 6H_2O$ in 5 mL water and 5 mL ethylene glycol. The combined solution was left to reflux overnight at 100 °C. A total of 11 washing steps were performed using varying ethanol-to-water ratios and small additions of NaOH to aid settling. A large amount of product was lost during washing, and the remaining powder had a yellow tint, indicating the washings were not successful.

Synthesis 5

In Synthesis 5, SnSe was synthesized first, and cobalt was introduced separately. For SnSe formation, Solution 1 contained 4.0093 g Se, 4.404 g $NaBH_4$, and 1.066 g NaOH in 100 mL of water. $NaBH_4$ was added incrementally when the solution turned dark. Solution 2 was prepared with 11.4655 g $SnCl_2 \cdot 2H_2O$ and 20 g NaOH in 300 mL of water. The two solutions were combined, forming a black precipitate, and the reaction was allowed to reflux overnight. The product was washed six times involving water and ethanol mixtures and yielded 9.553 g (95% yield), and later was found to be contaminated by iron from an unknown source. Three separate doping procedures were performed using this SnSe powder. In product 5.1, 0.2323 g of SnSe was combined with 0.0287 g of $CoCl_2 \cdot 6H_2O$ and 20 mL of water, then sealed in an autoclave and heated to 130 °C for 12 hours. Product 5.2 was prepared using 0.2383 g of SnSe and 0.0236 g of $CoCl_2 \cdot 6H_2O$ in 20 mL of water under the same autoclave conditions. Both produced clean powders. Product 5.3 involved 0.9989 g of SnSe, 0.12015 g of $CoCl_2 \cdot 6H_2O$, and 15 mL of ethylene glycol, which was autoclaved at 220 °C for 48 hours. This sample was degraded due to unintended contamination with ammonia and hydrogen peroxide.

Synthesis 6

Synthesis 6 was a revision of Synthesis 5. Solution 1 contained 0.993 g NaOH, approximately 4 g of $NaBH_4$, and 4.0233 g of Se in 100 mL of water. Solution 2 was composed of 11.495 g

$SnCl_2 \cdot 2H_2O$ and 20 g NaOH in 300 mL of water, and was heated to approximately 90 °C. Upon the addition of NaOH, the mixture changed from blue to black and then became clear. The two solutions were combined, and the reaction mixture was refluxed at 100 °C for 30 minutes. The precipitate was collected and washed, yielding 9.3781 g of clean product (93% yield).

Two doping attempts were made using this SnSe. For product 6.1, 2.0003 g of SnSe and 0.2402 g of $CoCl_2 \cdot 6H_2O$ were mixed in 40 mL of water. For product 6.2, 2.0002 g of SnSe and 0.1926 g of $CoCl_2 \cdot 6H_2O$ were used in the same volume. Both mixtures were split into two autoclaves (four in total), sealed, and heated at 130 °C for 80 hours. The resulting products were washed 8 times using ethanol-water mixtures. Both yielded clean powders: 6.1 gave 1.9199 g (96% yield) and 6.2 gave 1.926 g (96% yield) of final product.

3 Results & Discussion

3.1 Powder X-Ray Diffraction (XRD)

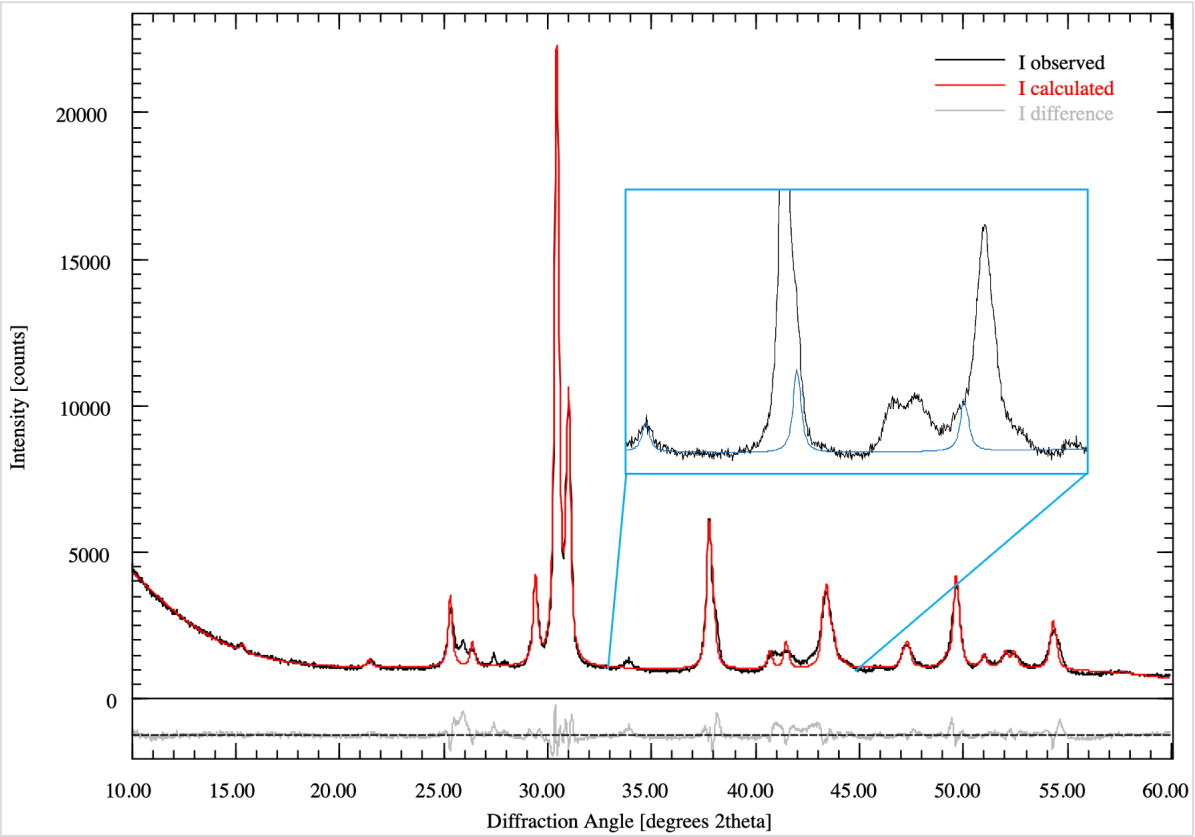

Figure 2: Powder XRD results of undoped SnSe (Synthesis 6).

Powder XRD was used to evaluate the purity, lattice parameters, and phases of the undoped and cobalt-doped SnSe samples. Le Bail refinement was chosen over Rietveld refinement, as the main purpose of the analysis was to determine whether there were any differences between the lattice parameters of the samples. Quantitative phase fractions cannot be determined with Le Bail refinement, although this was not deemed necessary, as secondary phases were present in minimal amounts.

The XRD pattern of the undoped SnSe sample from Synthesis 6 matches well with the reference pattern of orthorhombic SnSe (space group Pnma) as can be seen in Figure 2. The refinement fit closely follows the observed data. SnO_2 was considered as a secondary phase, the main indicator being the peak around 34°, the contribution of which is shown in blue. There are two more peaks that could not be explained definitively, in the 26-28° range, although they are observed in multiple measurements over various samples, indicating potential contaminants in reagents. One potential contaminant is SiO_2, although this could not be verified. These results indicate that the synthesis of SnSe was successful, with relatively low amounts of secondary phases.

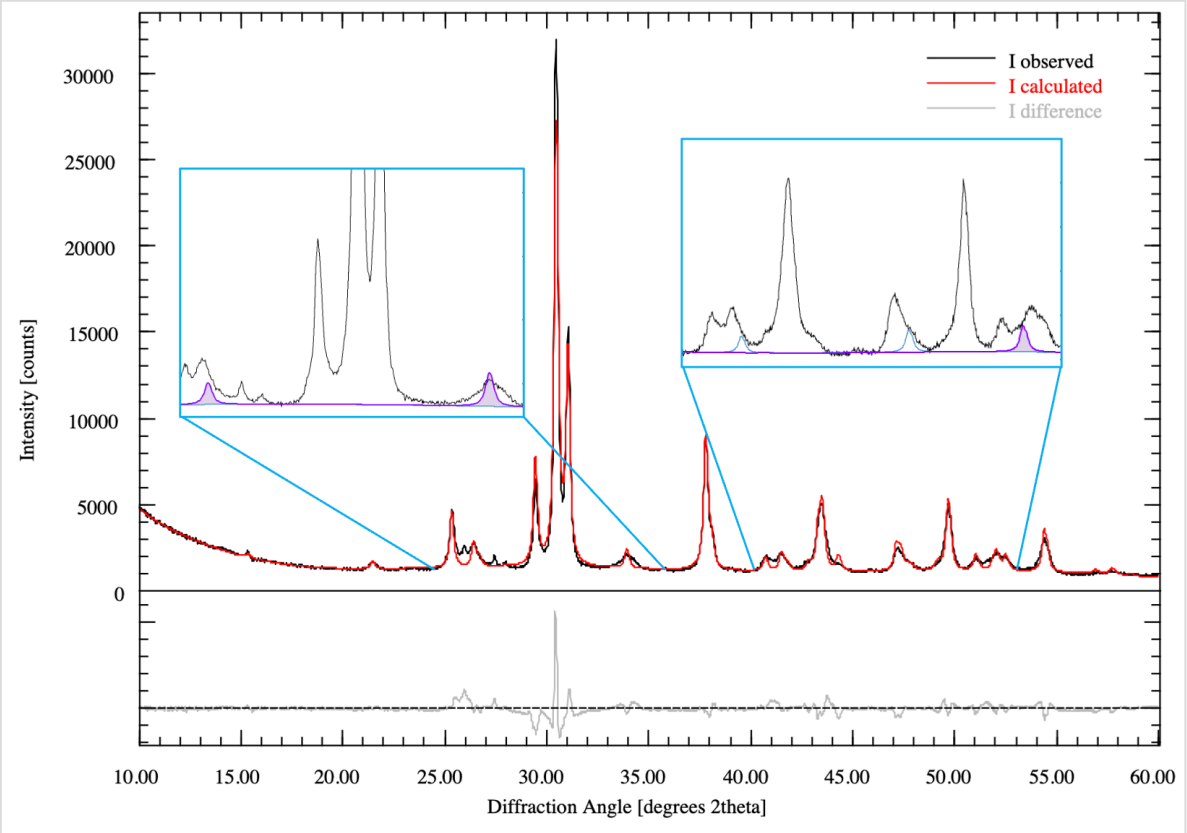

Figure 3: Powder XRD results of 10% Co-doped SnSe (Synthesis 6.1).

Figure 3 illustrates the similarity of the undoped and doped samples. As in Sample 6, SnO_2 peaks are seen and are shown in purple. In addition to these, there is a minor secondary phase of elemental cobalt (P63/mmc) shown in the close-ups by a blue line. It is difficult to confirm the presence or identity of all the phases, due to low intensity, and there are multiple possibilities: various tin, selenium, and cobalt compounds.

In Figure 4, the XRD spectrum of the Co-doped Sample 6.2 can be seen. There are no significant differences between the two doped samples. SnO_2 and Co secondary phases are present.

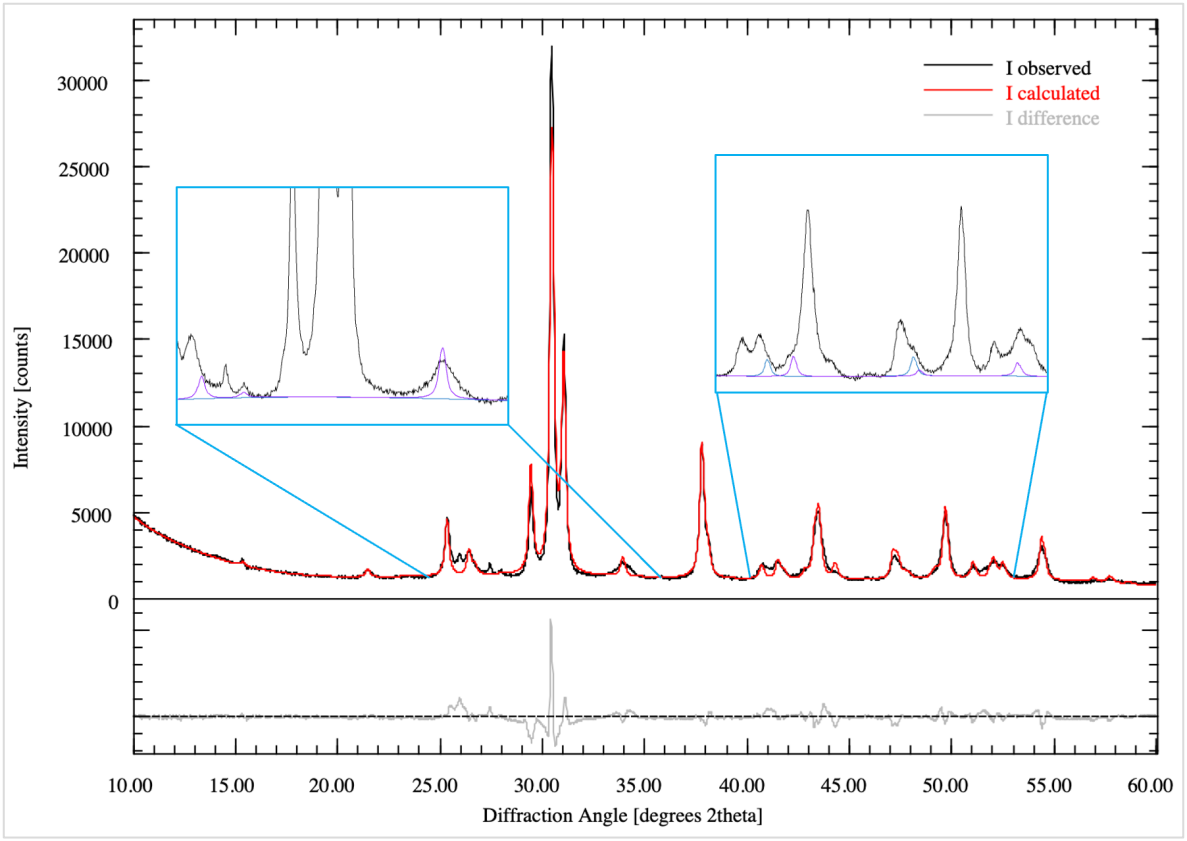

Figure 4: Powder XRD results of 8% Co-doped SnSe (synthesis 6.2).

The XRD results are summarized in Table 2 and compared with literature values for orthorhombic SnSe (Pnma) reported by Sist et al.[11] The lattice parameters obtained for the undoped sample (6 SnSe) were a = 11.5147(2) Å, b = 4.15684(8) Å, and c = 4.42337(8) Å, with a corresponding unit cell volume of 211.72 Å^3. These values are in agreement with the reported values (a = 11.4942 Å, b = 4.1510 Å, c = 4.4418 Å), although there is minor variation, mostly in the values of a and c. The a parameter is expected to vary more than the other parameters due to the van der Waals bonding between chains of SnSe. The small increase in the c-axis and unit cell volume may result from microstructural strain, differences in synthesis conditions, and impurities.

Table 2: Unit cell parameters.

Sample	Doping level (%)	a (Å)	b (Å)	c (Å)	Volume (Å^3)	Rwp (%)	Additional phases
Lit. SnSe[11]	0	11.49417	4.15096	4.44175	211.924	-	
6 SnSe	0	11.5147(2)	4.15684(8)	4.42337(8)	211.72357	8.32	Minor tin oxide
6.1 Co-SnSe	10	11.5176(2)	4.15761(6)	4.42947(7)	212.10822	7.74	Minor tin oxide and cobalt
6.2 Co-SnSe	8	11.5193(2)	4.15868(6)	4.42918(7)	212.18023	7.59	Minor tin oxide and cobalt

Interestingly, a slight unit cell expansion was observed upon cobalt doping, contrary to expectations based on ionic radii considerations. Sn^{2+} ionic radius in literature is given as 1.12 Å,[12] while cobalt ionic radius varies between 0.55 Å and 0.90 Å, depending on the environment and oxidation state.[5] The expected oxidation state of doped cobalt was 2+, with CN = 6, which has an ionic radius of 0.65 Å. Based on this, direct exchange with Sn^{2+} would be expected to cause unit cell contraction, which contradicts the XRD results. The 10% Co-doped sample (6.1 Co-SnSe) showed a unit cell volume of 212.11 $Å^3$, while the 8% doped sample (6.2 Co-SnSe) reached 212.18 $Å^3$, which are both larger than the undoped sample. This systematic volume expansion suggests that cobalt is most likely present in SnSe lattice holes and vacancies, introducing lattice strain. SnSe is known to be capable of handling crystal distortions, making it more plausible. Explaining the individual cell parameter differences is difficult, as SnSe can tolerate a significant amount of crystal distortions, which depend on many variables. In general, the doped samples might have a larger volume due to the additional autoclave step, during which the powder was kept at 130°C for 80h, potentially oxidizing some Sn^{2+} ions and introducing vacancies. This hypothesis could be tested using a control sample containing only SnSe and water during the autoclave step.

As mentioned before, minor secondary phases were identified in the doped samples, including tin oxide (SnO_2) and cobalt compounds. These impurities likely arise from residual precursors or byproducts of the doping treatment, though their intensities were low and did not significantly interfere with the refinement quality. Additionally, the presence of elemental cobalt suggests that a redox reaction may have occurred.

3.2 Scanning Electron Microscopy (SEM)

SEM results illustrate the irregular microplate-like structure of SnSe, which is consistent with expectations from the hydrothermal synthesis method. As shown in Figure 5, the SnSe crystals tend to cluster, and the particle shapes vary from irregular spheres to rods and plates. There is also considerable variation in grain size across all samples, as indicated by the large standard deviations reported in Table 3. The average grain size ranges from 180 nm in undoped SnSe to 200 nm in the 10% Co-doped sample. However, this is likely an underestimate, since larger grains - clearly visible in the SEM images - were difficult to isolate and measure. No significant morphological differences between doped and undoped samples were observed, suggesting that cobalt incorporation does not alter the crystal structure at this scale.

Table 3: SEM grain size analysis

Sample	Average Grain Diameter (nm)	Standard Deviation (nm)
6 SnSe	180	120
6.1 Co–SnSe	190	100
6.2 Co–SnSe	200	110

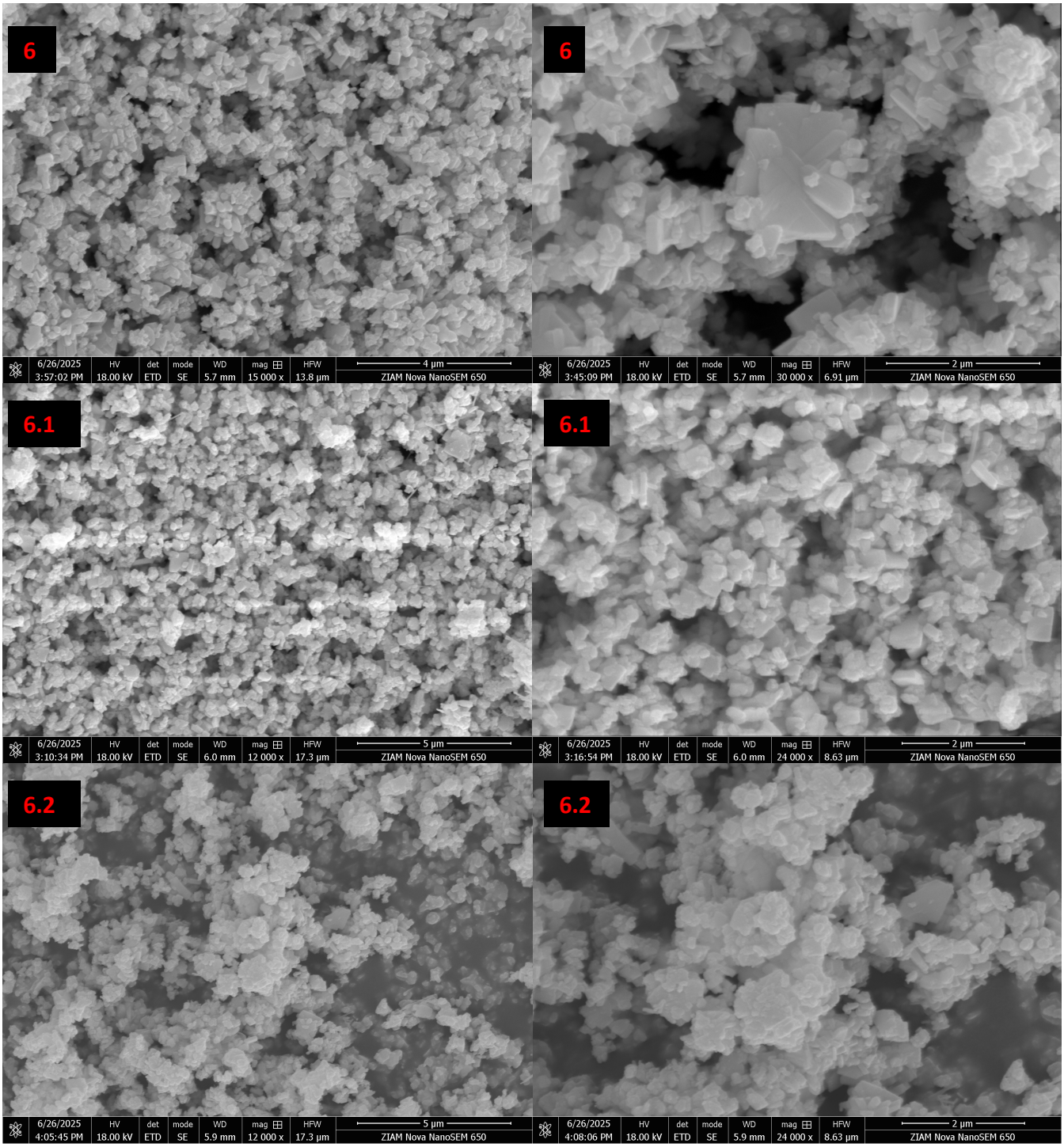

Figure 5: SEM images of Synthesis 6 products.

3.3 Energy-Dispersive X-Ray Spectroscopy (EDAX)

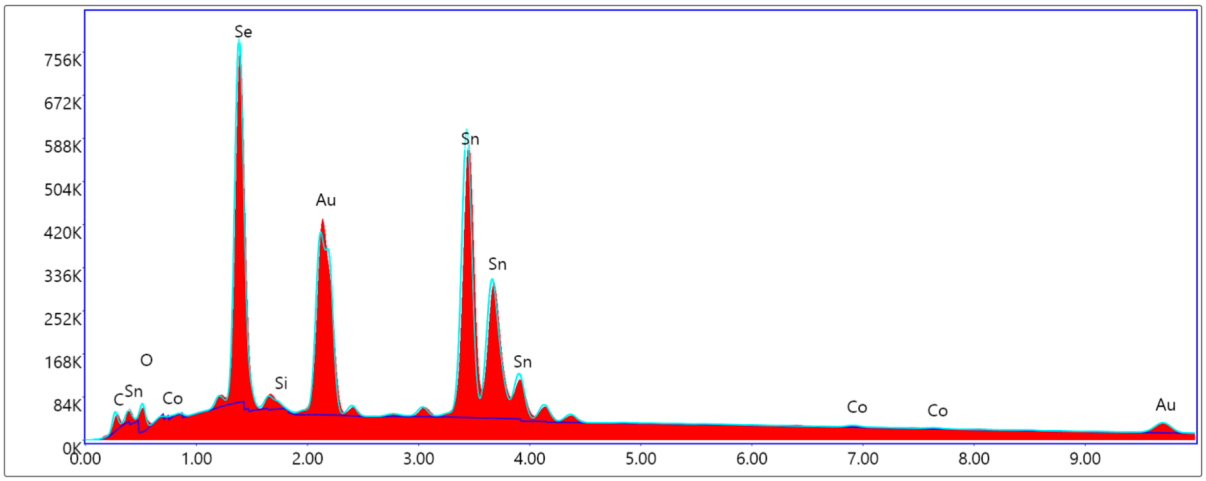

Figure 6: EDAX spectrum of 6.1 Co-SnSe.

Table 4: Semi-quantitative EDAX results of the 6.1 Co-doped SnSe sample.

Element	Weight %	Atomic %	Net Intensity	Error %
O K	2.01	11.57	60.20	8.43
Se L	28.29	33.04	783.50	5.28
Si K	0.29	0.94	14.80	8.36
Sn L	68.74	53.40	1214.70	1.82
Co K	0.67	1.05	8.60	8.76

EDAX was performed to verify the elemental composition of one of the cobalt-doped SnSe samples, namely Sample 6.1. Mapping of different samples could not be performed due to time constraints. Figure 6 shows the EDAX spectrum obtained from the chosen area, while Table 4 summarizes the quantitative values. The spectrum confirms the presence of Sn, Se, Co, and, in addition, O, Si, C, and Au. Carbon and gold were present due to the measurement method, while silicon seems to be a minor contaminant in all samples. Oxygen presence is most likely due to SnO_2, but could also be attributed to small amounts of cobalt oxides or tin hydroxides.

The values of Table 4 indicate that the sample predominantly consists of Sn (53.40%) and Se (33.04%), although the values deviate from the expected 1:1 or 0.9:1 ratio. This can be explained by the formation of tin oxides, as the oxygen atomic percentage is significantly higher than expected, approximately 11.57%. Cobalt is present in a small quantity (1.05%), showing that the doping method incorporates a fraction of the available cobalt atoms. It is worth mentioning that since EDAX is a semi-quantitative technique, the values should be considered as rough estimates.

Elemental mapping, shown in Figure 7, provides further insight into the distribution of the elements within the sample. Tin has a relatively homogeneous distribution, while selenium has a lower concentration in certain areas. Those areas seem to give a stronger signal of oxygen, further supporting the conclusion that tin oxide was formed in the sample, depleting selenium in those regions. Furthermore, the silicon distribution appears to follow the pattern of selenium, suggesting that the contamination might be due to the selenium precursor used in the synthesis. Notably, cobalt distribution, shown in Figure 8, seems homogeneous, which would be expected if cobalt were doped into the lattice. If cobalt atoms were present as secondary phases, concentrated regions would be seen in the mapping, unless cobalt clusters are evenly distributed throughout SnSe and are nanoscale, below the resolution of EDAX.

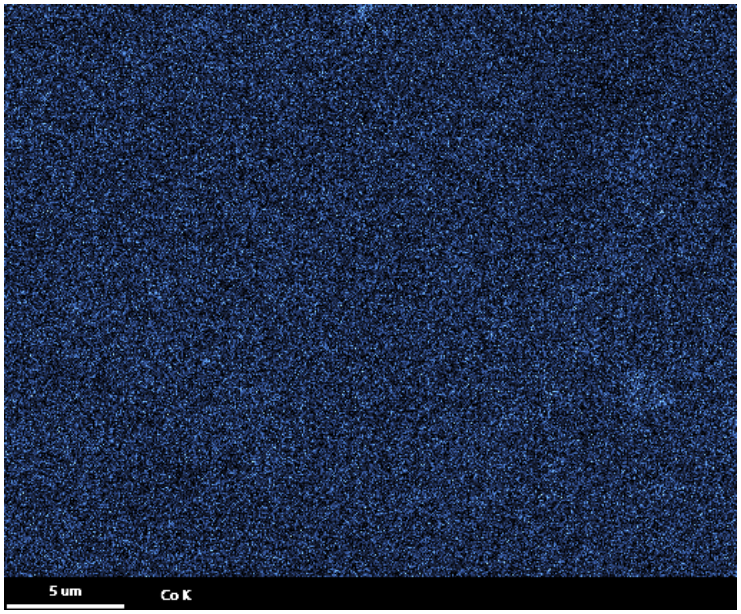

Figure 8: Cobalt distribution in Sample 6.1, Co-doped SnSe.

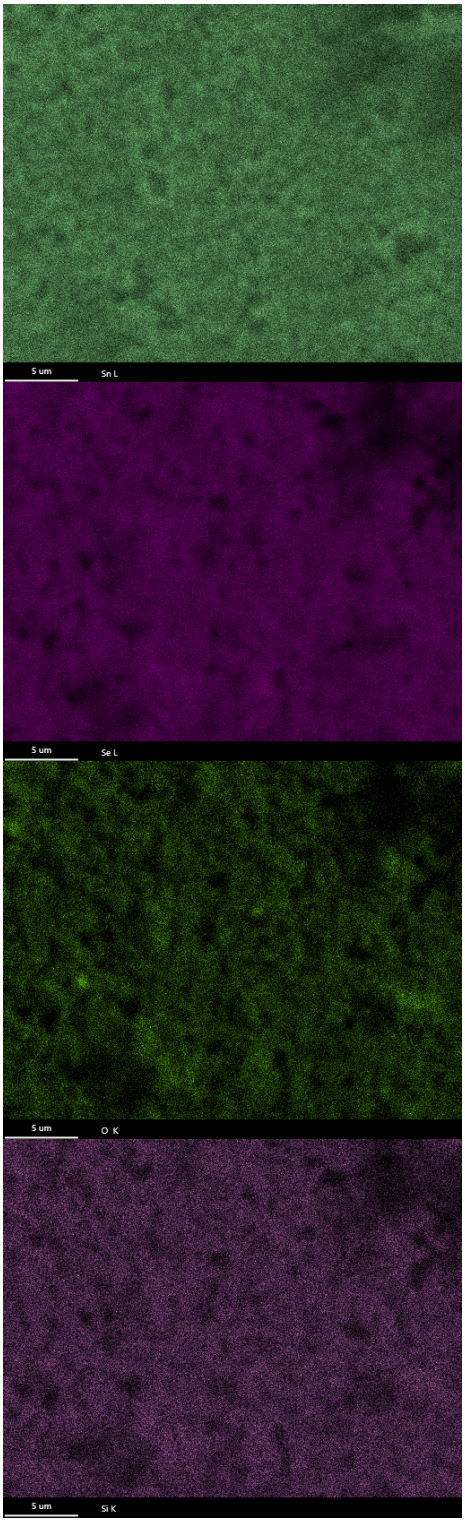

Figure 7: EDAX mapping of Sample 6.1 Co-doped SnSe.

3.4 Vibrating-Sample Magnetometry (VSM)

Magnetic measurements were performed on all the samples of Synthesis 6, including pure SnSe, and the two Co-doped samples, 6.1 and 6.2. Both temperature-dependent and field-dependent measurements were analyzed.

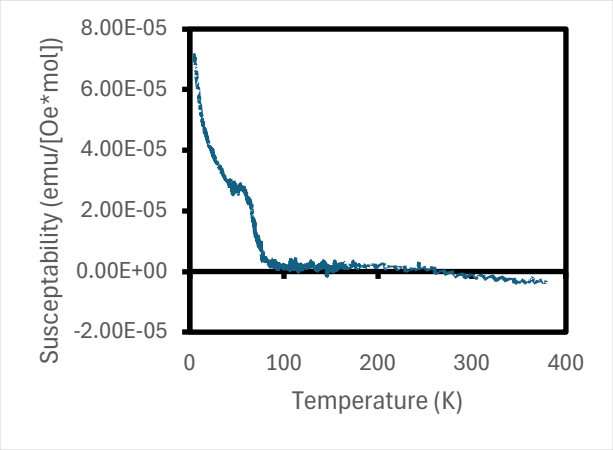

Figure 9: Susceptibility versus temperature measurement of Sample 6, at 90000 (Oe).

Figure 9 shows the susceptibility versus temperature curve for the undoped SnSe sample. The expected pattern is seen in the range of 80 - 380 K, where the susceptibility is approximately zero and constant, after diamagnetic corrections. This indicates that in this temperature region, only diamagnetic properties are measured. As SnSe does not have unpaired electrons, it should behave as a diamagnet, showing temperature-independent susceptibility. Notably, the sample deviates from this trend below 80 K, where an increase in susceptibility is seen. One potential explanation is that minor ferromagnetic impurities were present in the sample, although the susceptibility values are consistently low over the range of the measurement, thus, the concentration is low. The diamagnetic properties of SnSe were also expected to be observed in susceptibility versus field measurements, which are shown in Figure 10a. Notably, fast scans of all the samples showed no hysteresis and no saturation, therefore, for further measurements, a 0 to 90000 (Oe) sweep was performed to save measurement time. The susceptibility of sample 6 had strictly positive values and increased with the intensity of the field, again indicating low concentrations of a contaminant, potentially ferromagnetic. Together, these results confirm the diamagnetic characteristics of SnSe and indicate that some impurities were present during measurement.

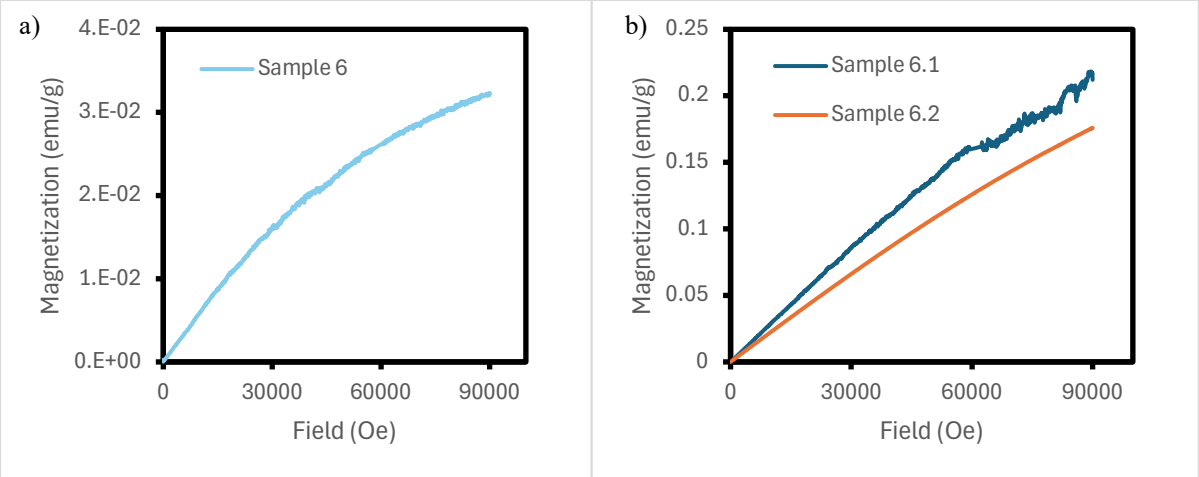

Figure 10: Magnetization versus field measurements of Synthesis 6 Samples. a) Undoped Sample 6, measured at 5 K. b) Co-doped samples 6.1 and 6.2, measured at 20 K.

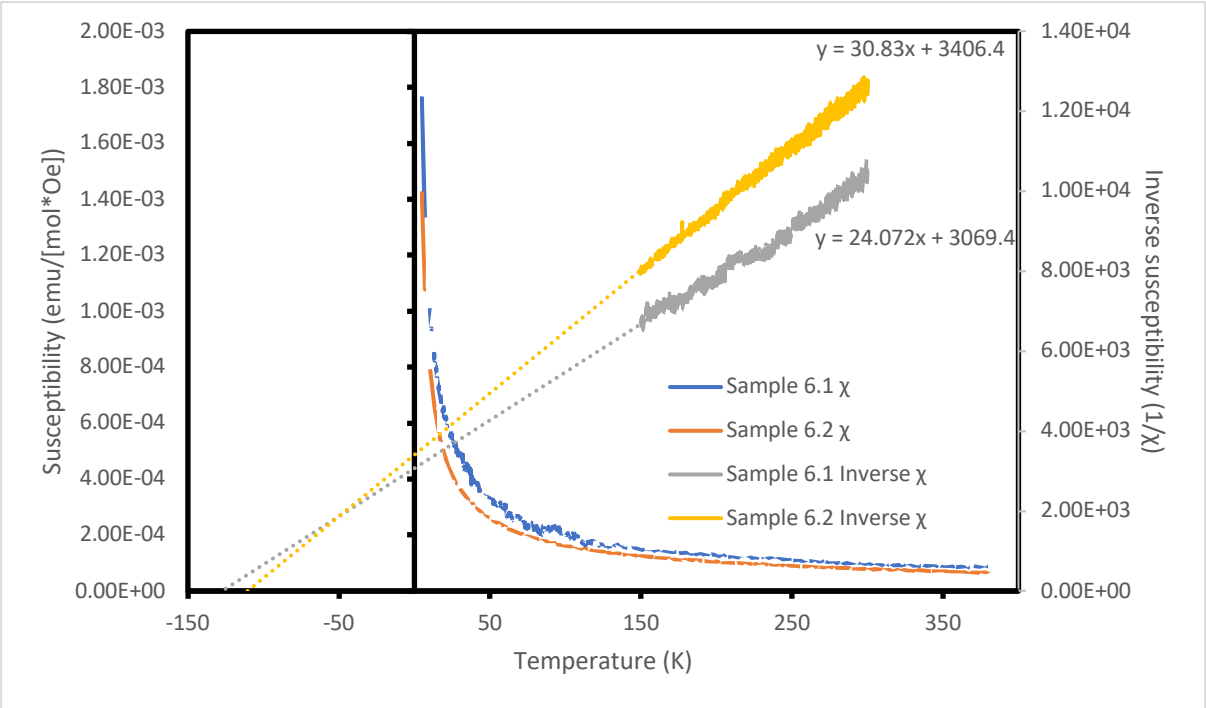

Figure 11: Susceptibility and inverse susceptibility versus temperature for Co-doped samples (Synthesis 6).

Figure 11 and Table 5 summarize the results for Co-doped samples 6.1 and 6.2. Between 150 and 300 K, both show Curie-Weiss-like behavior, with linear inverse susceptibility and negative Weiss temperatures, -128 K for Sample 6.1 and -110 K for Sample 6.2. The negative values suggest antiferromagnetic interactions between cobalt atoms, although no clear transition temperature was observed in the data, indicating that there is no long-range order in the samples. Furthermore, the effective moments were calculated: μ_{eff} (6.1) = 0.576μ_B, μ_{eff} (6.2) = 0.509μ_B. If cobalt is present in concentrations of 1-10%, the effective moment for cobalt is approximately 5 - 50 (μ_B). These values are significantly higher than the expected value for high-spin Co^{2+} (3.87μ_B)[9] or elemental Co (1.99μ_B),[13] which could be explained by superparamagnetism, where cobalt clusters behave as a single magnetic particle. AC magnetic measurements and TEM could be used to more precisely describe this behavior, although this was beyond the scope of this study. Notably, Sample 6.1 has a higher effective moment, showing that the solution concentration impacts the doping level, as expected.

Moment versus field measurements of doped samples were performed at 20 K and are shown in Figure 10b. As was mentioned before, hysteresis and saturation were not seen even at 90000 Oe, with the measured moment increasing non-linearly with field, indicating complex behavior. The steeper slope seen for Sample 6.1 is consistent with higher concentrations of cobalt. For Sample 6.1, the smooth curvature is disrupted at around 60000 Oe, possibly showing that the sample is approaching saturation.

Table 5: Summary of the magnetic measurements.

Sample	Curie Constant (emu*K/[mol*Oe])	Weiss Temperature (K)	Effective Moment (μ_B)
6.1	0.042	-128	0.58
6.2	0.032	-110	0.51

Considering Figures 10b and 11, the results seem to mirror the behavior of certain dilute magnetic semiconductors. A study of Co-doped ZnO found that their dilutely doped samples exhibit negative Weiss temperatures, no clear transition temperature, and curved magnetization response to changing field, which does not saturate and shows no hysteresis. The possible explanation given is that each cobalt ion only interacts antiferromagnetically with a few neighboring cobalt ions. Due to the concentration, there is no long-range order, giving a bulk paramagnetic response.[14] Another possibility is that the cobalt is incorporated as small nanoclusters of elemental cobalt. In that case, the cobalt clusters would give rise to superparamagnetic behavior, although measurements below 5K would have to be performed, as the blocking temperature was not observed. Additionally, XPS and ICP measurements would provide insight into the chemical state of Co, which would help explain the magnetic measurements.

4 Conclusion

In this study, the low-temperature hydrothermal synthesis of SnSe was optimized for Co-doping across six synthesis attempts. Findings suggest that ethylene glycol, in combination with $CoCl_2$, produces a significant amount of impurities that are difficult to wash, therefore, it is not suitable as a solvent. Additionally, doping SnSe hydrothermally after it has been washed further increases the purity of the final product. For this reason, only the products of Synthesis 6 were analyzed by XRD, SEM/EDAX, and VSM.

XRD data indicated relatively pure SnSe and the formation of Co^0 in the doped samples, while SnO_2 and an unidentified impurity were present in all of the samples. SEM images showed minimal differences between the samples in morphology and grain size. EDAX showed evenly distributed cobalt atoms, while the magnetic measurements revealed paramagnetic behavior and negative Weiss temperatures, suggesting antiferromagnetic interactions. The calculated effective moments were higher than typical values found in literature, suggesting superparamagnetism.

The combined results suggest that cobalt doping occurs not through direct substitution of Sn^{2+}, but via the formation of nanoscale elemental cobalt clusters.

In the future, other analytical techniques should be performed to quantify the results further. Namely, XPS for revealing the oxidation state of Co and the amounts of SnO_2 present, ICP for quantifying the doping level, TEM for potentially observing Co clusters, VSM below 5 K, and AC measurements for observing the blocking temperature and distinguishing between paramagnetic and superparamagnetic properties. Most importantly, thermoelectric measurements would reveal if the Figure of Merit can be improved with Co doping. Lastly, the synthesis method could be refined to produce a purer product and enable a more controlled doping level.

References

(1) Shi, X.; Tao, X.; Zou, J.; Chen, Z. High-Performance Thermoelectric SnSe: Aqueous Synthesis, Innovations, and Challenges. *Advanced Science* **2020**, *7* (7), 1902923. https://doi.org/10.1002/advs.201902923.

(2) Mukherjee, M.; Srivastava, A.; Singh, A. K. Recent Advances in Designing Thermoelectric Materials. *J. Mater. Chem. C* **2022**, *10* (35), 12524–12555. https://doi.org/10.1039/D2TC02448A.

(3) Zhang, P.; Lou, Z.; Gong, L.; Wu, Z.; Chen, X.; Xu, W.; Wang, Y.; Xu, J.; Dashevsky, Z.; Gao, F. Development and Applications of Thermoelectric Oxide Ceramics and Devices. *Energies* **2023**, *16* (11), 4475. https://doi.org/10.3390/en16114475.

(4) Nerella, M.; Suresh, M. B.; Bathulapalli, S. Room Temperature Ferromagnetism and Dielectric Properties of Cobalt Doped Tin Selenide for Spintronic Applications. *Physica B: Condensed Matter* **2022**, *627*, 413534. https://doi.org/10.1016/j.physb.2021.413534.

(5) Rahm, M.; Hoffmann, R.; Ashcroft, N. W. Atomic and Ionic Radii of Elements 1–96. *Chemistry A European J* **2016**, *22* (41), 14625–14632. https://doi.org/10.1002/chem.201602949.

(6) Diksha; Manyani, N.; Tripathi, S. K. Tuning Band Gap, Structural and Optical Properties of Tin Selenide Nanoparticles by Alkali Metal Doping. *Materials Today: Proceedings* **2023**, S2214785323008179. https://doi.org/10.1016/j.matpr.2023.02.273.

(7) Zhou, C.; Lee, Y. K.; Yu, Y.; Byun, S.; Luo, Z.-Z.; Lee, H.; Ge, B.; Lee, Y.-L.; Chen, X.; Lee, J. Y.; Cojocaru-Mirédin, O.; Chang, H.; Im, J.; Cho, S.-P.; Wuttig, M.; Dravid, V. P.; Kanatzidis, M. G.; Chung, I. Polycrystalline SnSe with a Thermoelectric Figure of Merit Greater than the Single Crystal. *Nat. Mater.* **2021**, *20* (10), 1378–1384. https://doi.org/10.1038/s41563-021-01064-6.

(8) Le Bail, A. Whole Powder Pattern Decomposition Methods and Applications: A Retrospection. *Powder Diffr.* **2005**, *20* (4), 316–326. https://doi.org/10.1154/1.2135315.

(9) Mugiraneza, S.; Hallas, A. M. Tutorial: A Beginner's Guide to Interpreting Magnetic Susceptibility Data with the Curie-Weiss Law. *Commun. Phys.* **2022**, *5* (1), 95. https://doi.org/10.1038/s42005-022-00853-y.

(10) Prasad, R.; Singha, S.; Sinha, P.; Saxena, S.; Vaidya, A.; Teli, S.; Saxena, U.; Harale, A.; Deshmukh, M.; Padvi, M.; Navathe, G. A Review on Modern Characterization Techniques for Analysis of Nanomaterials and Biomaterials. *ES Energy Environ.* **2024**, *10*, Article 1087. https://doi.org/10.30919/esee1087

(11) Sist, M.; Zhang, J.; Brummerstedt Iversen, B. Crystal Structure and Phase Transition of Thermoelectric SnSe. *Acta Cryst B* **2016**, *72* (3), 310–316. https://doi.org/10.1107/S2052520616003334.

(12) Stöwe, K.; Weber, M. Niobium, Tantalum, and Tungsten Doped Tin Dioxides as Potential Support Materials for Fuel Cell Catalyst Applications. *Z. Anorg. Allg. Chem.* **2020**, *646* (18), 1470–1480. https://doi.org/10.1002/zaac.201900345.

(13) Moon, R. M. Distribution of Magnetic Moment in Hexagonal Cobalt. *Phys. Rev.* **1964**, *136* (1A), A195–A202. https://doi.org/10.1103/PhysRev.136.A195.

(14) Guo, S.; Li, J.; Du, Z. Effect of Shallow Donors on Curie–Weiss Temperature of Co-Doped ZnO. *J. Magne. Magn. Mater.* **2014**, *371*, 49–51. https://doi.org/10.1016/j.jmmm.2014.07.041.